Catalog of *C*-Paired Spin-Momentum Locking in Antiferromagnetic Systems

Mengli Hu,[*] Xingkai Cheng, Zhenqiao Huang, and Junwei Liu[†]
Department of Physics, Hong Kong University of Science and Technology, Clear Water Bay, Hong Kong, China

(Received 18 August 2024; revised 27 February 2025; accepted 7 May 2025; published 5 June 2025)

Antiferromagnetic materials (AFMs) have been gaining lots of attention due to their great potential in spintronics devices and the recently discovered novel spin structure in the momentum space, i.e., *C*-paired spin-valley or spin-momentum locking (CSML), where spins and valleys or momenta are locked to each other due to the crystal symmetry guaranteeing zero magnetization. Here, we systematically study CSMLs and propose a general theory and algorithm using little cogroup and coset representatives, which reveals that 12 elementary kinds of CSMLs, determined by the geometric relation of spins and valleys and the essential symmetry guaranteeing zero magnetization, are sufficient to fully represent all possible CSMLs. By combining the proposed algorithm and high-throughput first-principles calculations, we predict 38 magnetic point groups and identify 142 experimentally verified AFMs that can realize CSML. Besides predicting new materials, our theory can naturally reveal underlying mechanisms of CSMLs' responses to external fields. As an example, two qualitatively different types of piezomagnetism via occupation imbalance or spin tilting are predicted in RbV_2Te_2O. The algorithm and conclusions can be directly extended to the locking between valley or momentum and any other pseudovector degree of freedom, e.g., Berry curvature, as exemplified in RbV_2Te_2O and the new proposed piezo-Hall effect, where a strain can induce a nonzero anomalous Hall conductance. In addition, the proposed concept and methodology can be straightforwardly applied to other symmetry groups, such as spin group.

DOI: 10.1103/PhysRevX.15.021083

Subject Areas: Condensed Matter Physics, Magnetism, Spintronics

I. INTRODUCTION

To access the spin degree of freedom (d.o.f.) of an electron, it is usually necessary to couple it with other d.o.f. such as the local magnetic moment via Zeeman interaction or angular momentum via spin-orbit coupling (SOC). The former supplies fertile ground for novel properties and applications of ferromagnetic materials (FMs). The latter has been the driving force of many intriguing phenomena in condensed matter physics and materials sciences in the past few decades, e.g., spin-valley locking (SVL) in two-dimensional materials [1], spin texture in topological materials [2,3], Rashba effect [4], and Dresselhaus effect [5] in semiconductors, which are also the underlying mechanism or building blocking of many thrilling discoveries such as valley Hall effect [1,6], spin Hall effect [7–10], giant spin-orbit torque [11–13], and Majorana zero modes [14–16]. These phenomena seem to be very different, while, besides SOC as their same origin, they do share the other same important feature, i.e., the contrasting spin polarization at time-reversal (*T*-) paired momenta due to the Kramers' theorem, and, hence, can be uniformly named as *T*-paired spin-valley or spin-momentum locking (SML). It also means that they will suffer from the same problems that spin can be manipulated only by approaches affecting the *T* symmetry. Consequently, materials with these properties cannot use spin d.o.f. to realize the nonvolatile information storage by themselves, which have become the bottlenecks hindering their practical applications. To overcome these problems, in 2021, SVL was extended to the antiferromagnetic systems (AFMs), where valleys or, in general, momenta with contrasting spin splitting are paired by a crystal (*C*) symmetry instead of the *T* symmetry, named *C*-paired SVL (CSVL) or SML (CSML) [17], which can come from the Pomeranchuk-type Fermi-surface instabilities in the spin channel [18] or generally exist in AFMs with spin-splitting band structures [17,19,20].

In CSML materials, any approach affecting the corresponding *C* symmetry can manipulate spin to induce unconventional phenomena [17,21–24]. Typically, a strain or electric field can introduce piezomagnetism (PZM)

[*]Present address: Institute for Theoretical Solid State Physics, IFW Dresden, Helmholtzstrasse 20, 01069 Dresden, Germany.
[†]Contact author: liuj@ust.hk

Published by the American Physical Society under the terms of the Creative Commons Attribution 4.0 International license. Further distribution of this work must maintain attribution to the author(s) and the published article's title, journal citation, and DOI.

[17,18] or noncollinear spin current (both spin-polarized current and pure spin current) in collinear AFMs as theoretically predicted [17,18,25,26] and experimentally confirmed in MnTe [27] and RuO_2 [28–30]. Besides these novel properties, the predicted spin-splitting band structures [17,19,20] and CSML [17] have been directly observed in angle-resolved photoemission spectroscopy in both collinear RuO_2 [31,32], MnTe [33,34] and CrSb [35–40], Rb/K intercalated V_2Te_2O [41] and V_2Se_2O [42], and noncollinear $MnTe_2$ [43,44]. Moreover, the electrical readout and deterministic 180° switching of the Néel order has also been realized in Mi_5Si_3 [45] and CrSb [46] thin films with or without assistant magnetic fields via manipulating the corresponding crystal symmetry [46], which further promotes applications of CSML AFMs in ultrafast, high-density, and highly stable devices.

To highlight their uniqueness, collinear CSML AFMs were named as altermagnet in 2022 [21,22], which has dramatically promoted the related study including all the experiments above and many other works. However, all these interesting phenomena above require neither collinear magnetic order nor the absence of spin-orbit coupling, and clearly altermagnet is only a subset of CSML AFMs. Similar terminology has been extended to the noncollinear spins in real space [47], while a thorough CSML theory in momentum space is still lacking and is in urgent need in understanding unconventional properties of CSMLs and exploring more CSML materials.

In this work, we developed a general and rigorous theory and algorithm to determine all the locked valleys or momenta with contrasting spin polarization, where the point operations in a magnetic space group (MSG) determine the allowed band splitting, the little cogroup of a momentum $\bar{G}^{\boldsymbol{k}}$ constrains the spin direction, and the coset representatives $\{g_m\}$ give rise to all the paired momenta with locked spins. We found that all CSMLs can be classified into three types—collinear, coplanar, or spatial—according to the direction of spins associated with the paired momenta; each type of CSML can be further categorized into four elementary families characterized by the symmetry guaranteeing zero magnetization in AFMs, and these 12 elementary kinds of CSMLs can serve as the building blocks of all CSMLs. Based on our theory and algorithm, 38 out of 122 MPGs were predicted to host CSML, and all possible symmetry-paired momenta and CSMLs are systematically enumerated, which indeed can be completely classified into the 12 elementary kinds as suggested by qualitative analysis. By combining with high-throughput first-principles calculations, 142 CSML materials were screened out of 1794 experimentally verified AFMs in MAGNDATA [48]. The full list can be found in Supplemental Material [49].

Besides cataloging all CSMLs and predicting new CSML materials, our theory is able to reveal the fundamental difference between symmetries in determining intrinsic properties of CSML materials, which distinguishes from and supplements the conventional symmetry analysis like Neumann's principle that treats all symmetries equally in the same way and, hence, can lead to unexpected conclusions. Typically, AFMs in the same MSG but with different CSMLs will have qualitatively different properties that are mainly determined by symmetries in little cogroup $\bar{G}^{\boldsymbol{k}}$ or the coset representatives $\{g_m\}$ but not other symmetries in MSG, which also corresponds to two qualitatively different underlying mechanisms, respectively. Our theory also reveals the importance of Fermi surface, which is critical for many phenomena but usually absent in the conventional symmetry analysis. We take Rb intercalated V_2Te_2O as a representative to show its two different types of PZM via either occupation imbalance determined by $\{g_m\}$ or spin tilting determined by $\bar{G}^{\boldsymbol{k}}$, which are not distinguished by conventional PZM theories based on the magnetic moments' rotation in real space but can be understood naturally in our new theory.

It is worth noting that the existence of valley d.o.f. is not a requirement for any results or conclusions above but will only add additional ingredients to the system and lead to new phenomena like valley (Hall) current, and the spin can be any pseudovector d.o.f. This is further exemplified by the Berry curvature distribution of RbV_2Te_2O as shown later. Based on the C-paired locking between Berry curvature and valleys or momenta, we proposed a new piezo-Hall effect, where a strain can break the C symmetry ensuring the exact Berry curvature-momentum locking to induce a nonzero net Berry curvature and, hence, a finite anomalous Hall conductance. Without any calculations, we can also conclude that the new proposed piezo-Hall effect can generally exist in any CSML materials once spin-orbital coupling or noncollinear magnetic order is considered, and this effect can also come from two kinds of mechanisms determined by symmetries in little cogroup $\bar{G}^{\boldsymbol{k}}$ or the coset representatives $\{g_m\}$, respectively, as in piezomagnetism.

II. GENERAL THEORY OF CSML

We first introduce the intuitive classification and criteria for CSMLs. Following the definition, SML can be intuitively classified into three different types—collinear, coplanar, and spatial (noncollinear and noncoplanar)—according to the relation of spin orientations of equivalent valleys as shown in Fig. 1, which can also be precisely obtained and identified by our SML algorithm as illustrated later.

Besides the apparent geometric meaning, the classification of three different types has clear physical implications and can directly reveal the qualitative responses of CSML AFMs to external fields. Taking spin current generation [17] as an example, the spin polarization of spin currents due to the collinear CSML [Fig. 1(a)] will be mainly along the z direction, while the spin polarization of spin currents

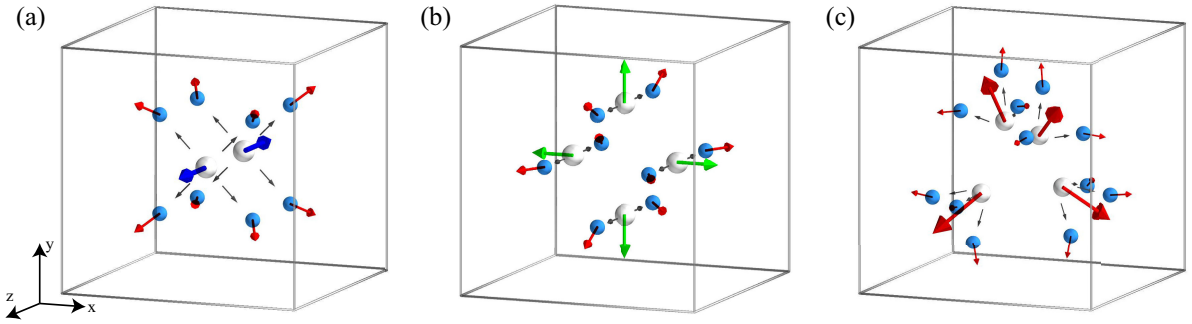


FIG. 1. Schematics of three types of CSMLs—collinear (a), coplanar (b), and spatial (c)—based on the geometric relation of orientations of spin at the paired valleys. White balls indicate the position of valleys in the Brillouin zone (BZ), and the associated arrows represent the corresponding spin orientation of the valley, which can be collinear, coplanar, or spatial (noncollinear and noncoplanar). The blue balls and black arrows present the evolution between different types of CSMLs with one valley split into several valleys. (a) and (b) show collinear and coplanar CSML in the magnetic point group (MPG) 422. In (a), spins are along the z direction when the valleys are located at $(0, 0, \pm w)$; in (b), spins lie in the x–y plane with valleys at $(\pm u, 0, 0)$ and $(0, \pm u, 0)$. When the valleys deviate from the high-symmetry points, collinear (coplanar) CSML transforms to the spatial CSML as shown by the black arrows in (a) [(b)]. In the spatial CSML (c), the number of coupled valleys in MPG 23 triples with valleys no longer at (u, u, u) and its equivalent high-symmetry points.

due to the coplanar CSML [Fig. 1(b)] will be in the x–y plane. Straightforwardly, different types of CSMLs should be able to realized in the same AFMs depending on the positions of valleys, and the transition between different types of CSMLs can occur as the Fermi level E_f changes. For example, CSML will evolve from a collinear type into a spatial type or further into a coplanar type as depicted by the white and blue balls in Figs. 1(a) and 1(b), and, consequently, the spin polarization of generated spin current will change the direction from the z direction to the x–y plane. It is interesting that a direct transition between a collinear and a coplanar CSML cannot happen but have to go through a spatial CSML.

To rigorously investigate SML and its unconventional properties in AFMs without any prior approximation, one usually needs to consider MSG, since it takes into account all possible symmetry constrains and interactions including SOC and effect of noncollinear magnetic orders. However, only point operations (rotation, reflection, and inversion) of space group symmetries, together with the time-reversal operation, can pair momenta and constrain the associated spin orientation (detailed derivation in Supplemental Material, Sec. I A [49]). Hence, the simpler MPG instead of more complicated MSG would be enough or even better for studying SML and its corresponding properties. Similarly, if without SOC, the main properties associated with SML will be determined mainly by the spin point group instead of spin space group [50–54]. Noted that some MSGs with the same MPGs may have different results, since the little cogroup of the same momentum might be different for different MSGs even though the MPG is the same, while this will not introduce any new type of CSMLs; i.e., all the possible CSMLs for different MSGs with the same MPG are the same. More details can be found in Supplemental Material, Sec. II C [49].

The primary criterion for a material to exhibit CSML is the existence of spin-splitting band structures, which can naturally occur in magnetic materials due to exchange interactions between electrons and localized magnetic moments once parity (inversion) times time-reversal (PT) symmetry is broken [19,55,56]. Second, we focus on CSML and, hence, exclude MPGs that are compatible with TSML, since the main properties will be determined by TSML instead of CSML once it exists. TSML magnetic materials will be very similar to nonmagnetic (NM) materials in many aspects, because there is an effective time-reversal symmetry $\tilde{T}^2 = -1$; even the pure real time-reversal symmetry is broken due to the magnetic structure. For example, in AFMs with checkerboard and Néel order, T times fractional translation τ symmetry $\tilde{T} = T\tau$ can be preserved. The final criterion is that at least one symmetry except PT symmetry must exist to ensure valleys and spins strictly locked to each other, which is shown later, is actually the symmetry that guarantees the exactly zero net magnetization in AFMs and, hence, can be naturally realized in AFMs.

Based on these three criteria above, all the MPGs can be classified into five classes depending on the existence of spin-splitting band structures and different types of SML as shown in Fig. 2(a). The first class includes all 32 MPGs with PT symmetry, and all the bands in the whole BZ must be spin degenerate. The other four classes allow spin-splitting bands at a generic momentum. Among them, the second class is compatible with a nonzero magnetization and, hence, can realize FM, weak FM (canted AFM), or ferrimagnetism. Note that the total magnetization in these MPGs could be zero due to the magnetic anisotropy energy, and, hence, the rigorous SML can be also realized. However, it would be material dependent, and the spin-dependent properties would possess both FM and AFM

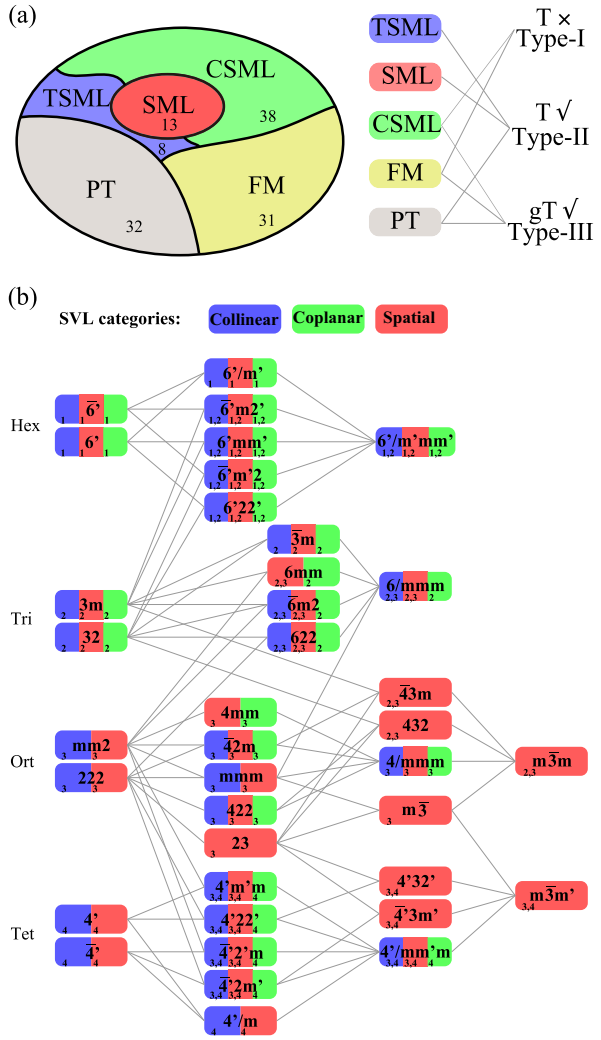


FIG. 2. (a) Diagram of MPGs with respect to SML. SML cannot exist in MPGs compatible with FM or PT symmetry. For all 59 MPGs compatible with SML, CSML can exist in 38 MPGs, TSML can exist in eight MPGs, and CSML and TSML can coexist in 13 MPGs labeled by SML. The full list of all MPGs can be found in Supplemental Material, Sec. I D [49]. The connection to the conventional classification [57–59] is shown in the right. (b) Inheritance of CSMLs among 38 CSML MPGs. The gray solid line connects a MPG and its subgroups. The background color denotes three types of CSML, and the numbers in the bottom left corner of each type represent the four elementary families. Hermann-Mauguin notation is used.

nature. Many experimentally realized altermagnets belong to this class due to a vanishingly small but finite magnetization and, hence, can realize an anomalous Hall effect that should be absent in perfect altermagnets or CSML materials. A simple example is a two-dimensional system that is compatible with MPG or MSG allowing out-of-plane net magnetization can be a perfect AFM if magnetic anisotropy energy favors the in-plane magnetic order and enforces an exact zero total magnetization. As a real material example, $CoNb_3S_6$ of MPG $32'$ is an AFM in experiment although MPG $32'$ is compatible with FM and allows a finite magnetization.

Based on the symmetries ensuring the zero magnetization and pairing equivalent momenta, the left MPGs can be classified into another three classes: 38 CSML MPGs as listed in Fig. 2(b) are due to crystal symmetries, eight TSML MPGs are due to (effective) time-reversal symmetry, and the left 13 MPGs are due to both crystal symmetries and time-reversal symmetry. It is worth noting that, except 38 CSML MPGs that must be realized in AFMs, the 21 MPGs hosting TSML and the 32 PT MPGs can exist in both AFMs and NMs. In this aspect, AFMs and NMs are indistinguishable in momentum space for 21 MPGs hosting TSML and 32 PT MPGs, and many of their properties are also qualitatively the same, which contrasts conventional understanding. As a result, one has to rely on the information or properties in real space and use MSGs to distinguish these AFMs and NMs.

A. SML algorithm and its application

Now we introduce the rigorous SML algorithm that can determine all the paired momenta and the orientation of associated spins. We found that two ingredients—the little cogroup of momentum $\bar{G}^{\boldsymbol{k}}$ and the coset representatives $\{g_m\}$—can fully capture and determine all the features of any SML with the former uniquely constraining the spin's orientation of the momentum $\boldsymbol{k}$ and the latter fully determining all the paired momenta and the associate spins' relation, respectively. The full SML algorithm consists of three steps:

(i) Get the MPG of a given AFM, labeled as $\bar{G}$.

(ii) For a momentum $\boldsymbol{k}$, find its little cogroup $\bar{G}^{\boldsymbol{k}}$ by checking if a element g in $\bar{G}$ satisfies $\boldsymbol{k} = g\boldsymbol{k} + \boldsymbol{K}$, where $\boldsymbol{K}$ is a reciprocal vector. CSML can exist only for momenta where spin splitting or spin polarization $\boldsymbol{s}$ is allowed, and the necessary and sufficient condition is that $\bar{G}^{\boldsymbol{k}}$ is compatible with FM, i.e., belongs to 31 FM MPGs as shown in Fig. 2(a) and listed in Supplemental Material, Sec. I D [49]; otherwise, such momenta will be spin degenerate and cannot realize SML.

(iii) All the paired momenta $\{\boldsymbol{k}^*\}$ and associate spins $\{\boldsymbol{s}^*\}$ can be obtained by $\{\boldsymbol{k}^*; \boldsymbol{s}^*\} = \{g_m\boldsymbol{k}; g_m\boldsymbol{s}\}$, where g_m is the representative of coset $g_m\bar{G}^{\boldsymbol{k}}$ and can be obtained via the coset decomposition $\bar{G} = \sum_m g_m\bar{G}^{\boldsymbol{k}}$. The matrix presentation of all g_m can be found in Supplemental Material, Sec. I C [49].

We applied this algorithm for all MSGs to enumerate all possible CSMLs and found that all CSMLs indeed belong to collinear (L), coplanar (P), or spatial (S) as shown in Fig. 1, which confirms the intuitive analysis above. The CSML type can be

rigorously determined based on $\bar{G}^{\boldsymbol{k}}$ without knowing other details as follows:

$$\forall\, \boldsymbol{k},\ \exists\, (-)N_{\boldsymbol{\alpha}} \in \bar{G}^{\boldsymbol{k}} \leftrightarrow L, \tag{2.1}$$

$$\forall\, \boldsymbol{k},\ \exists\, (-)N'_{\boldsymbol{\alpha}} \in \bar{G}^{\boldsymbol{k}} \rightarrow P, \tag{2.2}$$

$$\forall\, \boldsymbol{k},\ \exists\, (-)N_{\boldsymbol{\alpha}_k} \in \bar{G}^{\boldsymbol{k}}, \quad \boldsymbol{\alpha}_k \perp \boldsymbol{\alpha} \rightarrow P, \tag{2.3}$$

where $\boldsymbol{k} \in \{\boldsymbol{k}^*\}$, $-$ is the inversion operation, $N_{\boldsymbol{\alpha}}$ represents the N-fold rotation operation ($N > 1$) about the $\boldsymbol{\alpha}$ axis, and N' represents N-fold rotation times time-reversal symmetry. $\leftrightarrow$ denotes the necessary and sufficient, and $\rightarrow$ denotes the sufficient condition, respectively.

We take MPG $\bar{G} = 422$ (in Hermann-Mauguin notation) and momentum $\boldsymbol{k} = (0, 0, w)$ as an explicit example as shown in Fig. 1(a). Based on the generators (4_{001} and 2_{100}) of 422, the little cogroup of momentum $\boldsymbol{k} = (0, 0, w)$ can be easily obtained as $\bar{G}^{\boldsymbol{k}} = \{1, 4^+_{001}, 2_{001}, 4^-_{001}\} = 4$. Clearly, 4 is among 31 FM MPGs listed in Supplemental Material, Sec. I D [49], and belongs to FM; thus, CSML can exist. Then, via the coset decomposition $\bar{G} = \bar{G}^{\boldsymbol{k}} + 2_{100}\bar{G}^{\boldsymbol{k}}$, the coset representatives can be obtained as $\{g_m\} = \{1, 2_{100}\}$, which gives all the paired valleys and spins as $\{\boldsymbol{k}^*; \boldsymbol{s}^*\} = \{(0, 0, \pm w); (0, 0, \pm m_z)\}$, belonging to collinear CSML. The same conclusion can also be drawn by $\bar{G}^{\boldsymbol{k}}$, since the condition (2.1) is satisfied as $\forall\ \boldsymbol{k}, 4_{001} \in \bar{G}^{\boldsymbol{k}}$. Now we can obtain a counterintuitive conclusion that any magnetic materials with $\bar{G} = 422$ and valleys or momentum located at $\boldsymbol{k} = (0, 0, w)$ belong to collinear CSML even if their magnetic order in real space is noncollinear or noncoplanar, e.g., coplanar AFM $Ho_2Ge_2O_7$. The same procedure was conducted for all the valleys and momenta of 38 CSML MPGs, and the results are summarized in Fig. 2. Counterintuitively, a cubic crystal can allow only the spatial CSML, although it possesses the highest symmetry group. The reason is that cubic crystal hosts threefold rotational symmetries along body diagonals which violates all the conditions allowing collinear [Eq. (2.1)] or coplanar CSML [Eqs. (2.2) and (2.3)].

Besides enumerating all the CSMLs, our algorithm can rigorously capture the transition between different types of CSMLs, which can be described by another coset decomposition and is fully predictable. Taking the collinear CSML in Fig. 1(a) as an example, a momenta at $\boldsymbol{k} = (0, 0, w)$ splits into several general momenta, $\boldsymbol{k} = (0, 0, w) \rightarrow \boldsymbol{k}' = (u, v, w)$. Such a splitting can be described as $\bar{G}^{\boldsymbol{k}} = \bar{G}^{\boldsymbol{k}'} + 4^+_{001}\bar{G}^{\boldsymbol{k}'} + 2_{001}\bar{G}^{\boldsymbol{k}'} + 4^-_{001}\bar{G}^{\boldsymbol{k}'}$, which tells that each momentum splits into four momenta paired by the coset representatives as $\{\boldsymbol{k}'^*; \boldsymbol{s}'^*\} = \{\boldsymbol{k}', 4^+_{001}\boldsymbol{k}', 2_{001}\boldsymbol{k}', 4^-_{001}\boldsymbol{k}'; \boldsymbol{s}', 4^+_{001}\boldsymbol{s}', 2_{001}\boldsymbol{s}', 4^-_{001}\boldsymbol{s}'\}$ and the CSML transits from the collinear type into the spatial type. As a thorough summary of all the CSMLs of 38 MPGs in Fig. 2, one can predict and design CSMLs and the transition accordingly.

B. Elementary family of CSML

Although all CSMLs can be completely enumerated by our SML algorithm above, the connection between CSMLs of different MPGs is still unclear. Typically, some types of CSMLs exist only in a subgroup but *not* in its parent group and vice versa as shown in Fig. 2, which stems from a simple fact that the little cogroup of a subgroup is not necessarily a subgroup of the little cogroup of its parent group. Such an inconsistency also means that the classification merely using three different types cannot fully uncover the relation of all CSMLs.

To address this inadequacy, we carefully examined all the CSMLs enumerated by our SML algorithm above and found that (i) MPGs that can host CSMLs have at least one subgroup as $\bar{6}'/6'$, 3m/32, mm2/222, and $4'/\bar{4}'$, which are also four families of the smallest groups compatible with AFMs to guarantee the zero net magnetization, and, hence, we define these MPGs as four families of elementary CSML MPGs. (ii) The four families of elementary CSML MPGs correspond to four different crystal families—hexagonal, trigonal, orthorhombic, and tetragonal crystals, respectively. (iii) CSMLs that can be realized in these four families of elementary CSML MPGs come from the simplest $\bar{G}^{\boldsymbol{k}}$ and $\{g_m\}$ and have the smallest number of paired valleys and momenta. (iv) For any collinear and coplanar CSML, the symmetry axes in $\{g_m\}$ and $\bar{G}^{\boldsymbol{k}}$ must be orthogonal or parallel, and symmetries in $\{g_m\}$ and $\bar{G}^{\boldsymbol{k}}$ can be broken separately or simultaneously in orthogonal CSMLs but must be broken simultaneously in parallel CSMLs. Meanwhile, both orthogonal and parallel CSMLs can exist in the same system whose $\{g_m\}$ and $\bar{G}^{\boldsymbol{k}}$ can be broken separately. (v) Most importantly, a complicated CSML with more paired valleys or momenta that can be realized in other MPGs can always be taken as multiple copies of the simplest CSMLs realized in the elementary CSML MPGs. Based on these discoveries, we propose four elementary families of CSMLs as a new dimension and feature to describe all the CSMLs.

Together with three different types proposed above, 12 elementary kinds of CSMLs listed in the table in Fig. 3(a) can completely characterize and serve as building blocks for all the CSMLs as also indicated by the subscript numbers in the left bottom corner of each type of CSMLs in 38 CSML MPGs in Fig. 2. They can be concretely labeled as $F - T^{N_1(')}_{N_2(')} - R$, where $F =$ Hex, Tri, Ort, or Tet stands for the hexagonal, trigonal, orthorhombic, or tetragonal family, respectively, and $T = L$, P,

(a)

	Collinear	Coplanar	Spatial
Hex	$L^3_{6'}$-Para	$P^{2'}_{6'}$-Para	$S_{6'}$-Para
Tri	L^3_2-Orth	P^2_3-Orth	$S_{3,2}$-Orth
Ort	L^2_2-Orth	P^2_4-Orth	$S_{2,2}$-Orth
Tet	$L^2_{4'}$-Para	$P^2_{4'}$-Orth	$S_{4'}$-Para

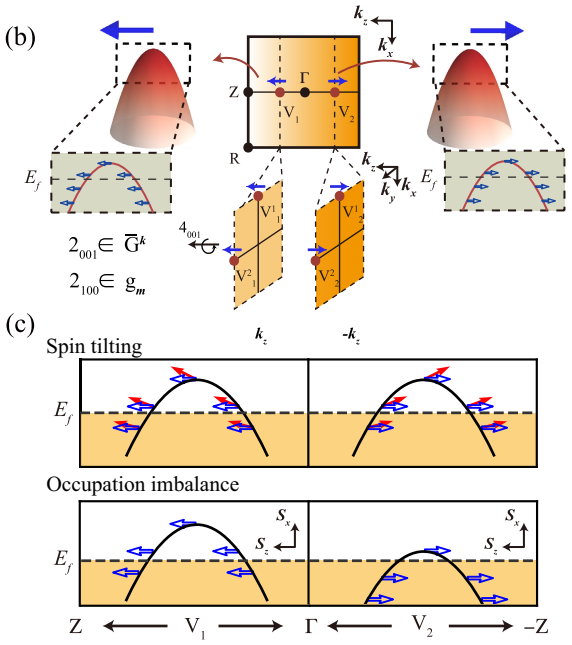


FIG. 3. (a) Table of 12 elementary kinds of CSMLs. Four elementary families of CSMLs are labeled by the abbreviation of hexagonal, trigonal, orthorhombic, and tetragonal, and different types of CSMLs with each elementary family are labeled by $L/P/S^{N_1(')}_{N_2(')}$, where $N_{1/2}(')$ labels the $N_{1/2}$-fold rotational symmetry in the $\bar{G}^{\boldsymbol{k}}$ and $\{g_m\}$, respectively. (b) Illustration of Ort-L^2_2-Orth kind CSML in MPG 422. The band structures around the valleys $V_{1/2}$ located at $(0,0,\pm w)$ and spins along z are presented. In the lower panel, the same kind CSML located at $(0,\frac{1}{2},\pm w)$ and $(\frac{1}{2},0,\pm w)$ are shown. Both CSML cases are paired by symmetry $2_{100}/2_{010}$ for their same CSML kind, and symmetry 4_{001} merely doubles the number of paired valleys by generating another copy (V^2) of the elementary CSML (V^1) but does not introduce any new property. (c) Two qualitatively different mechanisms generating PZM in Ort-L^2_2-Orth: spin tilting presented by a red filled arrow (top) and occupation imbalance reflected by the relative different Fermi levels of the valleys (bottom).

or S means collinear, coplanar, or spatial type, respectively, the superscript $N_1(')$ and subscript $N_2(')$ represent generators in $\bar{G}^{\boldsymbol{k}}$ and $\{g_m\}$, and $R =$ Orth or Para means orthogonal or parallel, respectively, between rotation axes of $N_1(')$ and $N_2(')$. Note that, for a more compact notation, the suffix $-R$ can be removed, since the 12 elementary kinds can belong to only either Orth or Para but not both.

Now it is clear that it is the elementary family instead of the geometric relation of spins' orientation inherited between different CSML MPGs as shown in Fig. 2. For example, MPG 432 can realize only the spatial-type CSMLs, while it can realize both trigonal and orthorhombic CSMLs, since its subgroups contain 32 and 222. On the contrary, although $4/mmm$ can realize all collinear, coplanar, and spatial types of CSMLs, it can realize only orthorhombic CSML, because its subgroups contain only $mm2/222$ but not other elementary CSML MPGs. This inheritance relation between elementary CSMLs and more complicated CSMLs can be also rigorously described by another coset decomposition as $\bar{G} = \sum_r g_r \bar{G}^E$, where $\bar{G}^E$ is the elementary CSML MPG and $\{g_r\}$ are coset representative. The symmetries in $\{g_r\}$ will only generate additional copies of the elementary CSMLs determined by $\bar{G}^E$ but not introduce too much new physics. As exemplified by the collinear CSMLs in 422 as shown in Fig. 3(b), a complicated collinear CSML with four different valleys or momenta at $k = (0,\frac{1}{2},\pm w)$ and $(\frac{1}{2},0,\pm w)$ are paired by $2_{100}/2_{010}$ and 4_{001}, while only $2_{100}/2_{010}$ can flip the direction of spins and enforce the opposite spin polarization for valleys or momenta at $k = (0,\frac{1}{2},\pm w)$ or $(\frac{1}{2},0,\pm w)$ and the 4_{001} symmetry merely generates another copy of the elementary CSML paired by $2_{100}/2_{010}$, i.e., Ort-L^2_2-Orth CSML in MPG 222, which can be rigorously obtained by the coset decomposition $422 = 222 + 4_{001}222$. Therefore, the collinear CSML in 422 will have the same property as the elementary Ort-L^2_2-Orth CSML in MPG 222. Breaking the symmetry 4_{001} will simply reduce the number of paired valleys or momenta from four to two, and only the symmetry $2_{100}/2_{010}$ matters for the unconventional properties arisen from CSMLs.

More importantly, without any complicated symmetry analysis and calculation, the elementary CSML has already been able to capture the main properties of AFMs arisen from CSMLs. To elucidate this more clearly, we take PZM as an example. In the example of collinear CSMLs in 422 and 222 that are Ort-$L^{N_1(')}_{N_2(')}$-Orth CSML, they belong to orthogonal CSMLs, which means the symmetries in $\bar{G}^{\boldsymbol{k}}$ and $\{g_m\}$ are orthogonal to each other and can be broken separately to realize two qualitatively different types of PZM. As illustrated in the top in Fig. 3(c), breaking symmetry in $\bar{G}^{\boldsymbol{k}}$ will induce spin tilting for all the valleys and momenta to induce uncompensated net magnetization, although different valleys and momenta are still equivalent due to $\{g_m\}$, and the direction of net magnetization will depend on $\{g_m\}$ and, hence, be in the x–y plane for the case in Fig. 3(c). This is like the conventional PZM due to local magnetic moments' nonequivalent rotation under strain [60] in real space, but it occurs in momentum space for spin of itinerant electrons associated with different valleys or momenta. On the other hand, as breaking symmetry in $\{g_m\}$, the strain will break the equivalence of different valleys and momenta to induce different energy

shifts and, hence, lead to unequal occupation of spin-up and spin-down electrons, and the net magnetization should be along the z direction, since spin orientation remains unchanged as shown in the bottom in Fig. 3(c). We refer to these two microscopic mechanisms as spin tilting and occupation imbalance, respectively, with the former driving AFM into weak FM (canted AFM) and the latter driving AFM into ferrimagnetism from the aspect of the real space. Notably, these two types of PZMs may coexist for certain strains, and both are qualitatively different from the conventional theory, since the nonzero net magnetization due to either spin tilting or occupation imbalance is from itinerant electrons instead of local magnetic moments [60] and, hence, can happen only in conducting AFMs.

In a short summary of our theory, with three different types and four elementary families as two independent features and dimensions, all CSMLs can be fully characterized and classified into 12 elementary kinds, and the main properties of CSML AFMs will be determined by the elementary CSMLs realized in these materials instead of other factors or material details.

III. APPLICATION AND MATERIAL REALIZATION

With the complete CSML theory and algorithm above, we employed the high-throughput first-principles calculations to predict CSML material candidates from the magnetic database MAGNDATA [48] and identified 142 CSML candidates with the experimentally confirmed desired magnetic structures. The full list of 142 CSML materials and their band structures along high-symmetry lines can be found in Supplemental Material, Sec. III [49].

In the following discussion, we choose Rb intercalated V_2Te_2O in our database as a representative, since it is one of the mostly studied AFMs now, and focus on its PZM which has not been fully studied. As shown in Fig. 4(a), RbV_2Te_2O belongs to the tetragonal crystal [41,61,62] and is a collinear AFM with Néel temperature higher than 300 K [41]. The local magnetic moments of V atoms are along the z direction, and two magnetic sublattices formed by different V atoms are connected by magnetic symmetry $\{4'_{001}|0\}$ and two diagonal mirror symmetry, which guarantee the perfect compensation and zero magnetization.

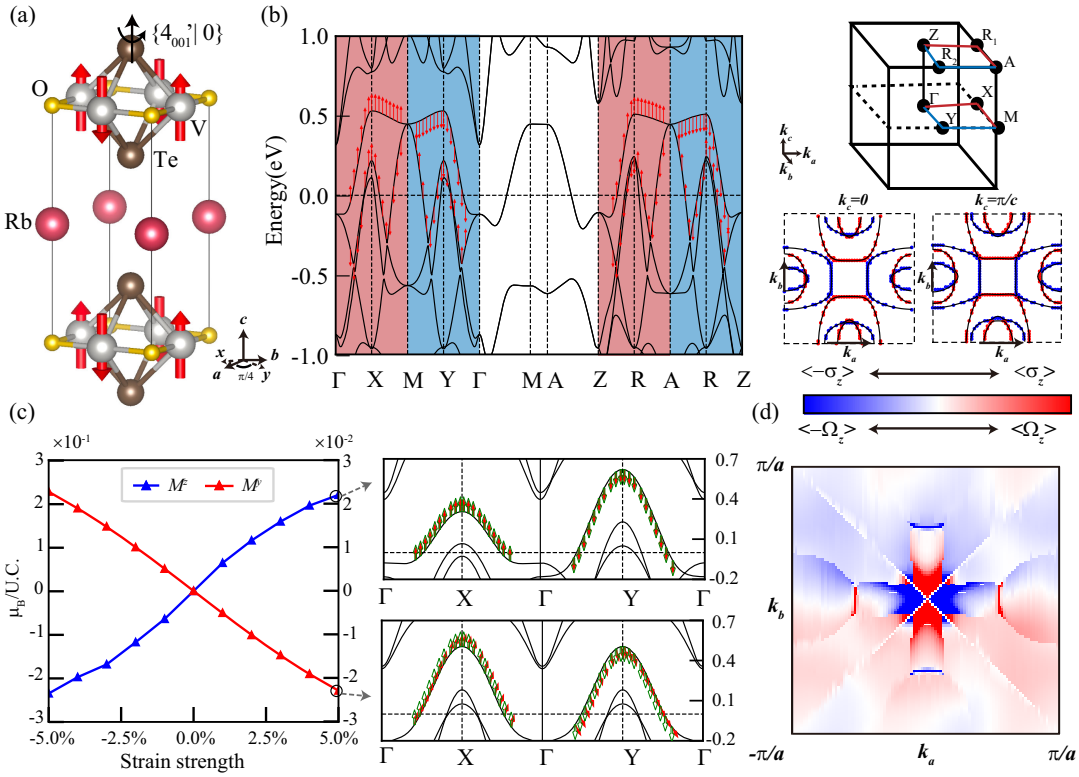


FIG. 4. A representative CSML material Rb intercalated V_2Te_2O. (a) Crystal and magnetic structure of RbV_2Te_2O, where the magnetic moments are labeled by red arrows. The Cartesian coordinate is anticlockwise rotated by $\pi/4$ of the unit vector along the $\boldsymbol{c}$ direction. (b) Band structure of RbV_2Te_2O along high-symmetry lines, where the region of coupled valleys is labeled by shadowed red and blue. The spin orientations of bands across Fermi level are denoted. The spin polarized Fermi surfaces are plotted in the lower right at $k_c = 0$ (left) and $k_c = (\pi/\boldsymbol{c})$ (right), respectively. The first BZ is shown in the upper right with high-symmetry points and corresponding spin polarization denoted. (c) Two types of PZM generated due to different mechanisms under two different kinds of strain $M^y = \Lambda^y_{xz}\sigma_{xz}$ and $M^z = \Lambda^z_{xx}\sigma_{xx}$. The strained valley band structures under +5% strain strength are shown in the right. The spin orientations without and with strain are labeled by solid red and hollow green arrows, respectively. (d) The Berry curvature(Ω) distribution in the first BZ with $k_c = 0$. The color map ranging from blue to red indicates the strength of Ω_z.

The adjacent magnetic layers share the same magnetic order, forming the C-type AFM, and its MPG is $\bar{G} = 4'/mm'm$.

As theoretically predicted and experimentally verified [17,41], RbV_2Te_2O is metallic with spin-splitting Fermi surfaces along $(\pm u, 0, v)$ and $(0, \pm u, v)$ as shown in Fig. 4(b). RbV_2Te_2O is a van der Waals layered material, and the dispersion along the z direction is almost unnoticeable; hence, we focus on $k_z = 0$ or $k_z = 0.5$ planes. The little cogroup at $k = (\pm u, 0, 0/0.5)$ and $(0, \pm u, 0/0.5)$ is $\bar{G}^{\boldsymbol{k}} = m'm2'$, and clearly $\forall\ \boldsymbol{k}, m \in \bar{G}^{\boldsymbol{k}}$, which satisfies the collinear condition (2.1). Together with Fig. 2, without any calculation of spin polarization, one can recognize that RbV_2Te_2O can realize the elementary CSML Tet-$L^2_{4'}$-Para and Ort-L^2_2-Orth, which is confirmed by the spin textures obtained by the first-principles calculations as denoted by red arrows in Fig. 4(b). As a result, RbV_2Te_2O can realize two different types of PZMs with spin tilting or occupation imbalance under different strains. To confirm it, two different types of strains σ_{xx} and σ_{xz} are considered, which can separately break either $\{g_m\}$ or $\bar{G}^{\boldsymbol{k}}$ in Ort-L^2_2-Orth and correspond to occupation imbalance or spin tilting, respectively. The results obtained by first-principles calculations with SOC considered are shown in Fig. 4(c). Both types of strain induce a net magnetization with the direction of magnetization and the microscopic mechanisms shown in the right in Fig. 4(c). Under the uniaxial stain σ_{xx} that only breaks the symmetry connecting different valley $\{g_m\}$ but maintains symmetries in little cogroup $\bar{G}^{\boldsymbol{k}}$, the spins are still along the z direction, but the occupation of spin-up and spin-down electrons are clearly imbalanced and, hence, the magnetization is strictly along the z direction, and the strained RbV_2Te_2O will behave like a ferrimagnet. On the contrary, a shear strain σ_{xz} can break $\bar{G}^{\boldsymbol{k}}$ but reserve $\{g_m\}$, and, hence, the spins around valleys all tilt from the z direction to the x–y plane, although two valleys are still equivalent under a shear strain σ_{xz}. As a result, the total magnetization will be in plane. In this case, the strained RbV_2Te_2O is more like a weak FM or tilted AFM. These uniaxial (σ_{xx}) and shear (σ_{xz}) strain-induced PZMs are consistent with previous study of linear symmetry-imposed PZM tensor [58,63], where the nonzero elements are $\Lambda^a_{ac} = \Lambda^a_{ca} = -\Lambda^b_{bc} = -\Lambda^b_{cb}, \Lambda^c_{aa} = -\Lambda^c_{bb}$, and $M^i = \Lambda^i_{jk}\sigma_{jk}$. Similar results and conclusions can also be explicitly demonstrated in KV_2Se_2O [42] and RuO_2 as shown in Supplemental Material, Sec. IV [49]. These results clearly confirm two different microscopic mechanisms of PZMs revealed by our general theory of CSMLs as explained in previous sessions and, hence, demonstrate the validity of our general theory and algorithm. Note that the symmetry of KV_2Se_2O is relatively high, and, hence, we can well separate the mechanism clearly. In general, the PZM tensor of a material with complex magnetic structure or lower symmetries may possess many nonzero independent components. In this case, both mechanisms may contribute to the overall PZM, and different nonzero independent components of PZM tensor may come from the same mechanism, either spin tilting or occupation imbalance. Determining the dominant contribution will depend on specific material properties like band structure changes under strain or the strength of spin-orbit coupling, which requires precise calculations that may exceed the capabilities of first-principles calculations and would be highly case dependent.

Since any pseudo-vector d.o.f. obeys the same transformation as spin under point symmetry operations, our theory and algorithm above can be directly applied to the locking between valley or momentum and any pseudovector d.o.f. Here, we use Berry curvature $\boldsymbol{\Omega}$ of RbV_2Te_2O as an example. This $\boldsymbol{\Omega}$-momentum locking phenomenon was first proposed in the TSVL 2H-MoS_2 [1] and is the origin of valley Hall effect [6]. Based on our CSML results, the $\boldsymbol{\Omega}$-momentum locking should be the same elementary kind, i.e., Tet-$L^2_{4'}$-Para and Ort-L^2_2-Orth. In addition, as $\bar{G} = \{\bar{G}^E, -1\bar{G}^E, 2_{110}\bar{G}^E, m_{110}\bar{G}^E\}$ and $\bar{G}^E = 4'$, there are four copies of $L^2_{4'}$ after the decomposition with respect to the elementary kind of CSML. The distribution of $\boldsymbol{\Omega}(k_x, k_y, 0)$ obtained by first-principles calculations is shown in Fig. 4(d), which indeed follows the prediction from our algorithm. These fan-shaped regions with same magnitude and alternating signs of Ω_z are four valleys belonging to $L^2_{4'}/L^2_2$ class, which will generate valley or spin Hall effect that are expected to reveal richer phenomena or properties of CSML materials. Importantly, as long as the AFM symmetry is strictly preserved, the total $\boldsymbol{\Omega}$ must be zero and the anomalous Hall effect is forbidden. However, the same as the PZM discussed above, a symmetry breaking induced by external strains will lead to nonzero net $\boldsymbol{\Omega}$ via either imbalanced occupation or $\boldsymbol{\Omega}$ tilting and, hence, the corresponding anomalous Hall effect, which can be referred to as a piezo-Hall effect. Besides, other approaches breaking the same crystal symmetries such as intrinsic distortions or finite magnetization due to Dzyaloshinskii-Moriya interaction can also generate net $\boldsymbol{\Omega}$ and the anomalous Hall effect.

IV. SUMMARY AND PERSPECTIVE

The new terminology altermagnet has attracted extensive attention and greatly promoted the study of spin-splitting AFMs or more broad unconventional magnetism. However, there are many inaccurate usages of altermagnet, which did not distinguish from canted AFMs and ferrimagnets and, hence, lead to many inaccurate conclusions, for example, whether an anomalous Hall effect can exist in altermagnets or not [24,64]. Compared to traditional study of magnetic materials focusing on real space, our theory shows that the key advances lie in the understanding of the spin structure in momentum space, e.g., CSML, where symmetries

involving crystal operations enforce a perfect locking between spin and momentum. It is worth emphasizing that CSML is fundamentally and intrinsically different from momentum-dependent spin splitting. In fact, spin splitting is always momentum dependent in any kind of materials as long as bands are not spin degenerate as in FMs, ferrimagnets, and even nonmagnetic materials with spin-orbit coupling or under external magnetic fields, and even the sign of such spin splitting can also be opposite at different momenta in these kinds of materials with suitable orbitals and interaction strengths. On the contrary, CSML can exist only in a perfect AFM or altermagnet but not any other materials. CSML ensures exact compensation of spin polarizations in momentum space and, hence, the exactly zero net magnetization but cannot lead to the exact cancellation of responses of spin-up and spin-down electrons to external fields as strain and electric fields, and, hence, CSML systems can have many FM-like responses even though the total magnetization is indeed zero, which fundamentally distinguishes from responses in ferrimagnets and canted AFMs. The differences among these concepts seem small but critical in the rigorous discussions of the novel properties of altermagnets.

With a focus on CSML, our work provides a unified and rigorous framework and algorithm to understand unconventional magnetism, which can be generally applied in all unconventional magnetism independent of whether the magnetic order is collinear and whether spin-orbit coupling is considered and can be extended to all spinlike pseudovector d.o.f. Although the number of all possible CSMLs seems to be very large or even infinite, we demonstrated that there are only 12 elementary kinds of CSMLs that can be rigorously defined by the geometric relation of spins and the essential symmetry guaranteeing the zero net magnetization. These 12 elementary kinds of CSMLs can capture all the new physics due to CSMLs and can serve as building blocks for all CSMLs. Our theory can easily and rigorously clarify many controversial conclusions. For example, we can conclude that a perfect altermagnet or CSML system intrinsically forbids the anomalous Hall effect, since Berry curvature follows the same rules as magnetization under symmetry operations, while the anomalous Hall effect can be induced by breaking the symmetry that leads to CSML via external strain or magnetic fields or internal Dzyaloshinskii-Moriya interaction, which effectively introduce a net magnetization and, hence, drive a perfect CSML system or altermagnet to a canted AFM or a ferrimagnet even though the net magnetization might be vanishingly small and does not contribute to the Berry curvature. Moreover, based on our theory, many new phenomena and properties of CSML materials can be predicted and understood, such as piezo-Hall effect, valley Hall effect, piezomagnetoelectric effect, and multiferroic effect, which can be experimentally verified and have potential applications in spintronics and valleytronics. The predicted 142 CSML materials as listed in Supplemental Material [49] and their properties will provide experimentalists more material platforms and may become a new research frontier in the field of magnetism, materials sciences, and condensed matter physics.

ACKNOWLEDGMENTS

This work is supported by National Key R&D Program of China (Grant No. 2021YFA1401500) and the Hong Kong Research Grants Council (16303821, 16306722, and 16304523).

[1] D. Xiao, G.-B. Liu, W. Feng, X. Xu, and W. Yao, *Coupled spin and valley physics in monolayers of* MoS_2 *and other group-VI dichalcogenides*, Phys. Rev. Lett. **108**, 196802 (2012).

[2] M. Z. Hasan and C. L. Kane, *Colloquium: Topological insulators*, Rev. Mod. Phys. **82**, 3045 (2010).

[3] X.-L. Qi and S.-C. Zhang, *Topological insulators and superconductors*, Rev. Mod. Phys. **83**, 1057 (2011).

[4] Y. A. Bychkov and É. I. Rashba, *Properties of a 2D electron gas with lifted spectral degeneracy*, JETP Lett. **39**, 78 (1984), http://jetpletters.ru/ps/1264/article_19121.pdf.

[5] G. Dresselhaus, *Spin-orbit coupling effects in zinc blende structures*, Phys. Rev. **100**, 580 (1955).

[6] K. F. Mak, K. L. McGill, J. Park, and P. L. McEuen, *The valley Hall effect in* MoS_2 *transistors*, Science **344**, 1489 (2014).

[7] J. Sinova, D. Culcer, Q. Niu, N. A. Sinitsyn, T. Jungwirth, and A. H. MacDonald, *Universal intrinsic spin Hall effect*, Phys. Rev. Lett. **92**, 126603 (2004).

[8] C. K. Safeer, J. Ingla-Aynés, F. Herling, J. H. Garcia, M. Vila, N. Ontoso, M. R. Calvo, S. Roche, L. E. Hueso, and F. Casanova, *Room-temperature spin Hall effect in* graphene/MoS_2 *van der Waals heterostructures*, Nano Lett. **19**, 1074 (2019).

[9] Y. Zhang, Y. Sun, H. Yang, J. Železný, S. P. P. Parkin, C. Felser, and B. Yan, *Strong anisotropic anomalous Hall effect and spin Hall effect in the chiral antiferromagnetic compounds* Mn_3X *(*X = Ge, Sn, Ga, Ir, Rh, *and* Pt*)*, Phys. Rev. B **95**, 075128 (2017).

[10] X. Chen, S. Shi, G. Shi, X. Fan, C. Song, X. Zhou, H. Bai, L. Liao, Y. Zhou, H. Zhang, A. Li, Y. Chen, X. Han, S. Jiang, Z. Zhu, H. Wu, X. Wang, D. Xue, H. Yang, and F. Pan, *Observation of the antiferromagnetic spin Hall effect*, Nat. Mater. **20**, 800 (2021).

[11] L. Liu, C.-F. Pai, Y. Li, H. W. Tseng, D. C. Ralph, and R. A. Buhrman, *Spin-torque switching with the giant spin Hall effect of tantalum*, Science **336**, 555 (2012).

[12] A. Manchon, J.Železný, I. M. Miron, T. Jungwirth, J. Sinova, A. Thiaville, K. Garello, and P. Gambardella, *Current-induced spin-orbit torques in ferromagnetic and antiferromagnetic systems*, Rev. Mod. Phys. **91**, 035004 (2019).

[13] S. Fukami, C. Zhang, S. DuttaGupta, A. Kurenkov, and H. Ohno, *Magnetization switching by spin-orbit torque in an*

antiferromagnet-ferromagnet bilayer system, Nat. Mater. **15**, 535 (2016).
[14] G. Moore and N. Read, *Nonabelions in the fractional quantum Hall effect*, Nucl. Phys. **B360**, 362 (1991).
[15] N. Read and D. Green, *Paired states of fermions in two dimensions with breaking of parity and time-reversal symmetries and the fractional quantum Hall effect*, Phys. Rev. B **61**, 10267 (2000).
[16] R. M. Lutchyn, E. P. A. M. Bakkers, L. P. Kouwenhoven, P. Krogstrup, C. M. Marcus, and Y. Oreg, *Majorana zero modes in superconductor-semiconductor heterostructures*, Nat. Rev. Mater. **3**, 52 (2018).
[17] H.-Y. Ma, M. Hu, N. Li, J. Liu, W. Yao, J.-F. Jia, and J. Liu, *Multifunctional antiferromagnetic materials with giant piezomagnetism and noncollinear spin current*, Nat. Commun. **12**, 2846 (2021).
[18] C. Wu, K. Sun, E. Fradkin, and S.-C. Zhang, *Fermi liquid instabilities in the spin channel*, Phys. Rev. B **75**, 115103 (2007).
[19] L.-D. Yuan, Z. Wang, J.-W. Luo, E. I. Rashba, and A. Zunger, *Giant momentum-dependent spin splitting in centrosymmetric low-Z antiferromagnets*, Phys. Rev. B **102**, 014422 (2020).
[20] S. Hayami, Y. Yanagi, and H. Kusunose, *Momentum-dependent spin splitting by collinear antiferromagnetic ordering*, J. Phys. Soc. Jpn. **88**, 123702 (2019).
[21] L. Šmejkal, J. Sinova, and T. Jungwirth, *Emerging research landscape of altermagnetism*, Phys. Rev. X **12**, 040501 (2022).
[22] L. Šmejkal, J. Sinova, and T. Jungwirth, *Beyond conventional ferromagnetism and antiferromagnetism: A phase with nonrelativistic spin and crystal rotation symmetry*, Phys. Rev. X **12**, 031042 (2022).
[23] L. Bai, W. Feng, S. Liu, L. Šmejkal, Y. Mokrousov, and Y. Yao, *Altermagnetism: Exploring new frontiers in magnetism and spintronics*, Adv. Funct. Mater. **34**, 2409327 (2024).
[24] C. Song, H. Bai, Z. Zhou, L. Han, H. Reichlova, J. H. Dil, J. Liu, X. Chen, and F. Pan, *Altermagnets as a new class of functional materials*, Nat. Rev. Mater. (2025).10.1038/s41578-025-00779-1
[25] R. González-Hernández, L. Šmejkal, K. Výborný, Y. Yahagi, J. Sinova, T. c. v. Jungwirth, and J. Železný, *Efficient electrical spin splitter based on nonrelativistic collinear antiferromagnetism*, Phys. Rev. Lett. **126**, 127701 (2021).
[26] M. Naka, S. Hayami, H. Kusunose, Y. Yanagi, Y. Motome, and H. Seo, *Spin current generation in organic antiferromagnets*, Nat. Commun. **10**, 4305 (2019).
[27] T. Aoyama and K. Ohgushi, *Piezomagnetic properties in altermagnetic* MnTe, Phys. Rev. Mater. **8**, L041402 (2024).
[28] A. Bose, N. J. Schreiber, R. Jain, D.-F. Shao, H. P. Nair, J. Sun, X. S. Zhang, D. A. Muller, E. Y. Tsymbal, D. G. Schlom, and D. C. Ralph, *Tilted spin current generated by the collinear antiferromagnet ruthenium dioxide*, National electronics review **5**, 267 (2022).
[29] H. Bai, L. Han, X. Y. Feng, Y. J. Zhou, R. X. Su, Q. Wang, L. Y. Liao, W. X. Zhu, X. Z. Chen, F. Pan, X. L. Fan, and C. Song, *Observation of spin splitting torque in a collinear antiferromagnet* RuO_2, Phys. Rev. Lett. **128**, 197202 (2022).
[30] S. Karube, T. Tanaka, D. Sugawara, N. Kadoguchi, M. Kohda, and J. Nitta, *Observation of spin-splitter torque in collinear antiferromagnetic* RuO_2, Phys. Rev. Lett. **129**, 137201 (2022).
[31] T. Berlijn, P. C. Snijders, O. Delaire, H.-D. Zhou, T. A. Maier, H.-B. Cao, S.-X. Chi, M. Matsuda, Y. Wang, M. R. Koehler, P. R. C. Kent, and H. H. Weitering, *Itinerant antiferromagnetism in* RuO_2, Phys. Rev. Lett. **118**, 077201 (2017).
[32] O. Fedchenko *et al.*, *Observation of time-reversal symmetry breaking in the band structure of altermagnetic* RuO_2, Sci. Adv. **10**, eadj4883 (2024).
[33] Kunitomi, Nobuhiko, Hamaguchi, Yoshikazu, and Anzai, *Shuichiro, Neutron diffraction study on manganese telluride*, J. Phys. (Paris) **25**, 568 (1964).
[34] J. Krempaský *et al.*, *Altermagnetic lifting of kramers spin degeneracy*, Nature (London) **626**, 517 (2024).
[35] J. Yuan, Y. Song, X. Xing, and J. Chen, *Magnetic structure and uniaxial negative thermal expansion in antiferromagnetic* CrSb, Dalton Trans. **49**, 17605 (2020).
[36] S. Reimers, L. Odenbreit, L. Šmejkal, V. N. Strocov, P. Constantinou, A. B. Hellenes, R. Jaeschke Ubiergo, W. H. Campos, V. K. Bharadwaj, A. Chakraborty, T. Denneulin, W. Shi, R. E. Dunin-Borkowski, S. Das, M. Kläui, J. Sinova, and M. Jourdan, *Direct observation of altermagnetic band splitting in* CrSb *thin films*, Nat. Commun. **15**, 2116 (2024).
[37] C. Li, M. Hu, Z. Li, Y. Wang, W. Chen, B. Thiagarajan, M. Leandersson, C. Polley, T. Kim, H. Liu, C. Fulga, M. G. Vergniory, O. Janson, O. Tjernberg, and J. van den Brink, *Topological Weyl altermagnetism in* CrSb, arXiv:2405.14777.
[38] J. Ding *et al.*, *Large band splitting in g-wave altermagnet* CrSb, Phys. Rev. Lett. **133**, 206401 (2024).
[39] M. Zeng *et al.*, *Observation of spin splitting in room-temperature metallic antiferromagnet* CrSb, Adv. Sci. **11**, 2406529 (2024).
[40] G. Yang *et al.*, *Three-dimensional mapping of the altermagnetic spin splitting in* CrSb, Nat. Commun. **16**, 1442 (2025).
[41] F. Zhang *et al.*, *Crystal-symmetry-paired spin-valley locking in a layered room-temperature metallic altermagnet candidate*, Nat. Phys. **21**, 760 (2025).
[42] B. Jiang *et al.*, *A metallic room-temperature d-wave altermagnet*, Nat. Phys. **21**, 754 (2025).
[43] P. Burlet, E. Ressouche, B. Malaman, R. Welter, J. P. Sanchez, and P. Vulliet, *Noncollinear magnetic structure of* $MnTe_2$, Phys. Rev. B **56**, 14013 (1997).
[44] Y.-P. Zhu *et al.*, *Observation of plaid-like spin splitting in a noncoplanar antiferromagnet*, Nature (London) **626**, 523 (2024).
[45] L. Han, X. Fu, R. Peng, X. Cheng, J. Dai, L. Liu, Y. Li, Y. Zhang, W. Zhu, H. Bai, Y. Zhou, S. Liang, C. Chen, Q. Wang, X. Chen, L. Yang, Y. Zhang, C. Song, J. Liu, and F. Pan, *Electrical 180° switching of Néel vector in spin-splitting antiferromagnet*, Sci. Adv. **10**, eadn0479 (2024).
[46] Z. Zhou, X. Cheng, M. Hu, R. Chu, H. Bai, L. Han, J. Liu, F. Pan, and C. Song, *Manipulation of the altermagnetic order in* CrSb *via crystal symmetry*, Nature (London) **638**, 645 (2025).

[47] S.-W. Cheong and F.-T. Huang, *Altermagnetism with non-collinear spins*, npj Quantum Mater. **9**, 13 (2024).

[48] S. V. Gallego, J. M. Perez-Mato, L. Elcoro, E. S. Tasci, R. M. Hanson, K. Momma, M. I. Aroyo, and G. Madariaga, *MAGNDATA: Towards a database of magnetic structures. I. The commensurate case*, J. Appl. Crystallogr. **49**, 1750 (2016).

[49] See Supplemental Material at http://link.aps.org/supplemental/10.1103/PhysRevX.15.021083 for 142 screened CSML materials and selected material band structures, derivation of SML, CSMLs with respect to different MPGs, MPG classification in terms of SML, PT, and FM, point symmetry matrix operations, and PZM calculation results for RuO_2.

[50] P. Liu, J. Li, J. Han, X. Wan, and Q. Liu, *Spin-group symmetry in magnetic materials with negligible spin-orbit coupling*, Phys. Rev. X **12**, 021016 (2022).

[51] Z. Xiao, J. Zhao, Y. Li, R. Shindou, and Z.-D. Song, *Spin space groups: Full classification and applications*, Phys. Rev. X **14**, 031037 (2024).

[52] J. Yang, Z.-X. Liu, and C. Fang, *Symmetry invariants and classes of quasiparticles in magnetically ordered systems having weak spin-orbit coupling*, Nat. Commun. **15**, 10203 (2024).

[53] W. Brinkman and R. J. Elliott, *Theory of spin-space groups*, Proc. R. Soc. A **294**, 343 (1966).

[54] D. B. Litvin and W. Opechowski, *Spin groups*, Physica (Utrecht) **76**, 538 (1974).

[55] S. Hayami, Y. Yanagi, and H. Kusunose, *Bottom-up design of spin-split and reshaped electronic band structures in antiferromagnets without spin-orbit coupling: Procedure on the basis of augmented multipoles*, Phys. Rev. B **102**, 144441 (2020).

[56] Y. Liu, J. Li, P. Liu, and Q. Liu, *Unconventional spin textures emerging from a universal symmetry theory of spin-momentum locking*, npj Quantum Mater. **9**, 69 (2024).

[57] W. H. Kleiner, *Space-time symmetry of transport coefficients*, Phys. Rev. **142**, 318 (1966).

[58] M. Seemann, D. Ködderitzsch, S. Wimmer, and H. Ebert, *Symmetry-imposed shape of linear response tensors*, Phys. Rev. B **92**, 155138 (2015).

[59] C. Bradley and A. Cracknell, *The Mathematical Theory of Symmetry in Solids: Representation Theory for Point Groups and Space Groups* (Oxford University, New York, 2009).

[60] A. S. Borovik-Romanov, *Piezomagnetism, linear magnetostriction and magnetooptic effect*, Ferroelectrics **162**, 153 (1994).

[61] A. Ablimit, Y.-L. Sun, E.-J. Cheng, Y.-B. Liu, S.-Q. Wu, H. Jiang, Z. Ren, S. Li, and G.-H. Cao, V_2Te_2O*: A two-dimensional van der Waals correlated metal*, Inorg. Chem. **57**, 14617 (2018).

[62] A. Ablimit, Y.-L. Sun, H. Jiang, S.-Q. Wu, Y.-B. Liu, and G.-H. Cao, *Weak metal-metal transition in the vanadium oxytelluride* $Rb_{1-\delta}V_2Te_2O$, Phys. Rev. B **97**, 214517 (2018).

[63] S. V. Gallego, J. Etxebarria, L. Elcoro, E. S. Tasci, and J. M. Perez-Mato, *Automatic calculation of symmetry-adapted tensors in magnetic and non-magnetic materials: A new tool of the Bilbao Crystallographic Server*, Acta Crystallogr. Sect. A **75**, 438 (2019).

[64] Q. Liu, X. Dai, and S. Blügel, *Different facets of unconventional magnetism*, Nat. Phys. **21**, 329 (2025).